Dry friction avalanches: Experiment and theory

Sergey V. Buldyrev,[1] John Ferrante,[2] and Fredy R. Zypman[1]
[1]*Department of Physics, Yeshiva University, 2495 Amsterdam Avenue, New York, New York 10033, USA*
[2]*NASA-Glenn Research Center, 21000 Brookpark Road, Cleveland, Ohio 44135, USA*
(Received 8 September 2005; revised manuscript received 21 June 2006; published 19 December 2006)

Experimental evidence and theoretical models are presented supporting the conjecture that dry friction stick-slip is described by self-organized criticality. We use the data, obtained with a pin-on-disk tribometer set to measure lateral force, to examine the variation of the friction force as a function of time. We study nominally flat surfaces of matching aluminum and steel. The probability distribution of force drops follows a negative power law with exponents μ in the range 3.2–3.5. The frequency power spectrum follows a $1/f^{\alpha}$ pattern with α in the range 1–1.8. We first compare these experimental results with the well-known Robin Hood model of self-organized criticality. We find good agreement between theory and experiment for the force-drop distribution but not for the power spectrum. We explain this on a physical basis and propose a model which takes explicitly into account the stiffness and inertia of the tribometer. Specifically, we numerically solve the equation of motion of a block on a friction surface pulled by a spring and show that for certain spring constants the motion is characterized by the same power law spectrum as in experiments. We propose a physical picture relating the fluctuations of the force drops to the microscopic geometry of the surface.

DOI: 10.1103/PhysRevE.74.066110 PACS number(s): 05.65.+b, 46.55.+d, 64.60.Ht

I. INTRODUCTION

There are experimental and theoretical studies suggesting that certain far-from-equilibrium systems with many degrees of freedom naturally organize in a critical state, releasing energy through rapid relaxation events (avalanches) of different sizes, these sizes being distributed according to a power-law probability density. Examples of such behavior are found in earthquakes [1,2], biological systems [3], the stock market [4], rainfall [5], and friction [6–8]. All these phenomena share the features of the prototypical sandpile model [9] for which the concepts of self-organized criticality (SOC) were first proposed. Recently, the possibility of SOC [10] in systems presenting stick-slip due to dry friction has been under scrutiny [11]. Experimental evidence of SOC in the stick-slip dynamics of two artificially constructed elastic surfaces with macroscopic asperities was presented in Refs. [12,13]. Slanina [6] presented theoretical attempts to explain dry friction in terms of SOC. However, the central question remains unanswered: to what extent is dry friction stick-slip a manifestation of SOC? The clarification of this issue has practical as well as fundamental implications. From the practical point of view, the power law exponents could be used as parameters to characterize the friction of surfaces. From the fundamental point of view, there is a growing interest to understand systems driven far away from equilibrium from a single unifying principle. Moreover, there is not yet a full understanding of the dissipation mechanisms in friction. Particularly, an overall description of the topography of the interface would be useful. In addition, there are claims that avalanches should not exist in dry friction [2]. We believe that the answer depends on experimental conditions. For example, with an atomic force microscope where the contact can be described reversibly, one would expect force drops commensurate with the underlying lattice structures of the tip and the sample. Indeed, there is experimental evidence that that might be the correct picture for friction at that scale [14]. Another example corresponds to dry friction between two surfaces with an intervening monolayer of a foreign material. In that case, it is possible for the monolayer to substantially reduce the strength of the interaction between surfaces and thus eliminate avalanches altogether. Here, we consider the interaction between two bare surfaces as commonly used in macroscopic dry friction. The goal is to clarify whether or not for these very general systems avalanches exist, the extent to which SOC is a possible underlying mechanism, and to gain a physical understanding of the critical state.

Friction is an extremely complex phenomenon, which involves microscopic interactions between two surfaces, comprising elastic interactions, nonelastic shear stress dissipation, mass, and energy transfer [15–17]. There are a number of models currently used to describe friction: (i) realistic *ab-initio* models [18–28] based on molecular dynamics, (ii) simplified models of motion of a single elastic tip in a periodic atomic potential known as Tomlinson models [14,29–34], (iii) models based on the driven elastic chain approximation [35–37], and (iv) discrete models of extremal dynamics such as the Slanina model [6].

With the fast increase of computational power, it has become possible to study friction by molecular dynamics simulations based on integrating Newton's equation of motion of atoms with classical approximations for interatomic interaction potentials [19]. This approach has been also used for studying scratching [20] and stick-slip motion of atomic force microscope (AFM) tips [21]. The questions asked in these studies cover fundamental problems of velocity, load, and temperature dependence of the friction force, mechanisms of energy dissipation [19,22], and asperity shear [23], as well as applied problems of how a particular organic monolayer coating [24,26] and hydrophobicity in the presence of water vapor [27] affect friction. These studies show that friction strongly depends on the commensurability of surfaces and their smoothness, with totally different mechanisms acting for rough surfaces (Coulomb law) and

atomically smooth surfaces (Stokes law) [28]. They also suggest that when friction does not involve wear, the stick-slip is periodic and the distribution of the slip magnitude distribution is narrow [19], while in the presence of scratching and irreversible atomic displacement [21] the behavior of the friction force is chaotic and has a wide distribution [20]. Although these models are very useful for the understanding of molecular mechanism of friction, they can model only very small systems limited to a fraction of a micron in length for a very short time intervals limited to a fraction of a microsecond. Obviously, macroscopic SOC behavior cannot fully develop on such small spatial and temporal scales.

Another theoretical approach to study friction is based on the Tomlinson model [14,29] which models the interaction between a single sliding object (representing, for example, an AFM tip) and a surface. The corresponding Newton equation is solved with a periodic potential intended to mimic the periodic structure of crystalline lattices in contact and a stochastic term modeling thermal activation. These models predict a relatively narrow Gaussian-like distribution of stick-slip forces, which is confirmed in the AFM experiments [30]. They also predict a power-law [31] or logarithmic increase of friction force with velocity [32,33] and vanishing of friction with temperature increase (thermolubricity)[34]. These models are not suitable to study SOC in dry friction because they have essentially one degree of freedom, which is the coordinate of the sliding object.

Very promising models of dry friction which show the evidence of SOC are the models based on a driven elastic chain which interact with a surface via a disordered potential consisting of randomly placed Gaussian bumps. In this model the surface motion is represented by an overdump motion of elastically coupled beads [35–37], connected by springs to an object representing a tribometer arm moving with a constant velocity along the surface. This model is one dimensional and does not involve any mass transfer. At small velocities, the distribution of the stick-slip drops, ΔF, is a power law $P(\Delta F) \sim \Delta F^{-\mu}$ with $\mu = 1.07$, which is a typical manifestation of SOC, which is in good agreement with the experimental studies of the stick-slip dynamics of artificially constructed elastic surfaces with macroscopic asperities [7] which find $0.8 < \mu < 2.0$ depending on the interface velocity. However, this value of μ is far from our experimental observations.

The driven elastic chain model is related to even simpler one-dimensional lattice models of extremal dynamics such as Zaitsev's Robin Hood model and Bak-Sneppen evolution model [38–40], which have similar power laws describing the avalanche size distribution and other properties some of which can be found analytically [41–43]. For this reason, oversimplified lattice models of extremal dynamics are still of value in understanding basic principles of friction in the same spirit that two-dimensional Ising-type models are paradigmatic in the studies of critical phenomena and phase transitions. In the extremal dynamics models, the distribution of avalanches reaching certain threshold of a critical parameter follows a power law with an exponent τ slightly larger than 1. The main problem in applying these models to real phenomena is relating their parameters to the real experimental observables. For example, Slanina defined a critical variable analogous to Bak-Sneppen fitness or a merchant's wealth in the Robin Hood model to be the amount of elastic energy accumulated in one asperity. However, the mapping of time steps and spatial jumps in his interpretation to a real dynamics remains problematic. He postulates that as the maximal stress exceeds certain threshold the surface jumps to a new location and the process of self-organization starts from the very beginning. This postulate apparently leads to a narrow stick-slip distribution, since the slip is always caused by almost the same amount of energy. On the other hand, he relates the stick-slip distribution to the events within a self-organization process, which seems to be inconsistent with his postulate. In addition, the distribution of jumps in his interpretation also decays as a power law with an exponent μ approximately equals to one.

Self-organized criticality is generally observed in systems with many degrees of freedom in which the external stress is slowly accumulating, while the system response takes place on a much shorter time scale in an avalanche type of activity during which a fraction of external stress is released. Such systems with two dramatically different time scales are usually called the extremal dynamics systems. The simplest way to model such systems is to use lattice models in the spirit of the invasion percolation [39], the sandpile model [9], Bak-Sneppen evolution model [40], and Zaitsev's Robin Hood model [38]. The theory of these models is rather well understood, and the behavior of their variables is characterized by several power laws with the exponents obeying well-established relations. As we mentioned above, the largest challenge is to relate the variables of the extremal dynamics models to the observables of the real dynamics. Once this relation is established the exponents of the extremal dynamics model may be compared with experiment.

For example, the exponent τ characterizing the distribution of avalanche sizes is usually assumed to be related to the exponent μ characterizing the distribution of the drops of the friction force. For example, in the sliding chain model [35] in which the relation between the extremal and real dynamics can be clearly established, an avalanche can be regarded as a period of motion during which the maximum velocity of the sliding beads exceeds the constant velocity of the driving mechanism. Suppose that during such period of activity s beads have been moving faster than the driving bar. Then the total reduction of the friction force ΔF scales as $\Delta F \sim s\langle \Delta x \rangle$, where Δx is an average displacement of the bead during such fast motion, which is the typical distance between the Gaussian-shape asperities. Accordingly, the force drop is proportional to the avalanche size s and the exponent μ must be identified with τ. In all known extremal dynamic models (one and two dimensional) $\tau \in [1,2]$. Our experimental results (Sec. II) give $\mu = 3.4 \pm 0.5$, so it is clear that the equivalence between the avalanche size and the drop in the friction force is not valid.

In this paper we propose another way of relating the parameters of an extremal dynamics model to the experimental observables which yields a better agreement with the experiment. Among several models of extremal dynamics one of the simplest and most elegant is the Robin Hood model, which was originally proposed for dislocation movement

[38] and later was adopted for modeling dry friction [6] by Slanina who added to the original Robin Hood model several parameters aimed to better capture the dry friction mechanism, but essentially obtained the same type of behavior as the original model. Here we return to the original Robin Hood model due to its simplicity.

In the present study, we consider statistical properties of the force drop experimentally (Sec. II) and theoretically (Sec. III). In Sec. IV we discuss the possible relevance of the dimensionality and elasticity in a theoretical description of friction models. In Sec. V we present the conclusions of our experimental and theoretical studies.

First (Sec. II), we present experimental results on stick-slip in dry friction using a pin-on-disk tribometer, set to measure lateral forces. The probability distributions of force drop sizes and the corresponding frequency power spectra for matching aluminum and steel couples are examined for evidence of SOC. Second (Sec. III), we attempt a theoretical explanation of the observed power laws based on the Robin Hood model [38] (Sec. III A in which we summarize previously known theoretical results and Sec. III B in which we relate to dry friction). Third, we extend the previous model (Sec. III C) to account for the finite stiffness and inertia of the real tribometer as is done in Tomlinson model with the difference that instead of periodic atomic forces we use power-law-distributed forces generated by the extremal dynamics mechanism as the microscopic input to the model.

The critical difference between our approach and that taken in the elastic chain approximation is that our friction mechanism is based on the assumption of nonelastic mass transfer between the asperities which is not taken into account by the elastic chain model. In Sec. III B we describe how we model the asperity interactions, using the critical variable "wealth" to represent the local distance between the surfaces rather than stress. Accordingly, we assume that random redistribution of wealth between neighboring merchants is equivalent to mass transfer. Thus our approach may be of particular relevance in the studies of wear friction. Our extremal dynamics model produces the distribution of the microscopic force drops which agrees well with the our experimental results. However, it fails to describe the spectral features of the experimentally recorded time series of the friction forces, which is not surprising since our extremal dynamics model neglects inertia and stiffness of the real macroscopic tribometer. That is why we explicitly introduce the tribometer via its elastic constant and mass as in Tomlinson models (Sec. III C). This is the second feature which distinguishes our work from previous attempts to model friction by extremal dynamics models. We use the nonelastic asperity interaction taken from the Robin Hood model as a noise-generating mechanism which serves as a microscopic input into a macroscopic tribometer represented by a massive object driven with constant velocity by an elastic spring as in Tomlinson model. This approach represents a combination between Robin Hood and Tomlinson models. We show that the macroscopic output of the extended model retains the power law distribution of the force drops but also reproduces the spectral features of our experiments.

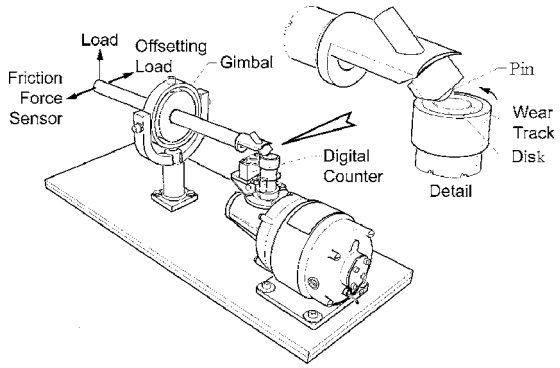

FIG. 1. Pin-on-disk tribometer. The arrow points at the location where the spherical pin and the disk touch. The disk lies horizontally while the pin attached to the arm rests above it.

II. EXPERIMENT

The pin-on-disk tribometer used for these experiments is shown in Fig. 1. This configuration was chosen because it allows for easy replacement of the contacting surfaces and it is the standard method for measuring friction and wear in unlubricated and lubricated contacts. The apparatus uses a 2.54-cm-diameter disk and a spherical pin with a 0.95 cm radius machined on its end. The pin is attached to a load arm that is mounted on a gimbal supported at the center through which a load applied at the end of the arm is transferred to the contact zone. A strain gauge is mounted at the end of the arm to monitor tangential friction force. The tangential force is monitored at a sample rate of 1000 scans/sec, and conversion is done using a 16-bit data acquisition card controlled by LABVIEW. Data are recorded to a text file for later analysis. Frictional force measurements are done on matching aluminum and steel (M50) pin-and-disk tribometers. The signal is collected at 1 kHz during 16 min, thus collecting 10^6 points. The first quarter of each data set, or about 4 min, is discarded to assure that a steady state is reached. In order to drive the system very slowly away from static equilibrium, we select slow rotational speeds in the range 10–20 rpm. Each disk is used for up to four tests by changing the radial position of the pin on the disk. Loads for aluminum range from 250 g to 1000 g. M50 steel is studied with a 1000-g normal load between pin and disk. Figure 2 shows a typical tangential friction force versus time trace. It shows force drops of various sizes.

We first construct the probability distribution of force drops. Force drops are taken as those events corresponding to negative changes in the tangential force. We next obtain the probability distributions of the tangential friction force drops corresponding to aluminum on aluminum under various loads and M50 on M50 steel. Results of such analysis are presented in Figs. 3–6. We observe an approximate linear behavior on the log-log plots suggesting a power law behavior of the distributions $P(\Delta F) \sim \Delta F^{-\mu}$ with exponents μ close to 3.

We also compute the power spectra of the tangential friction force time series. The power spectrum is, by definition, the modulus squared of the Fourier transform of the original time series. The power-law spectrum of a time series $F(t)$

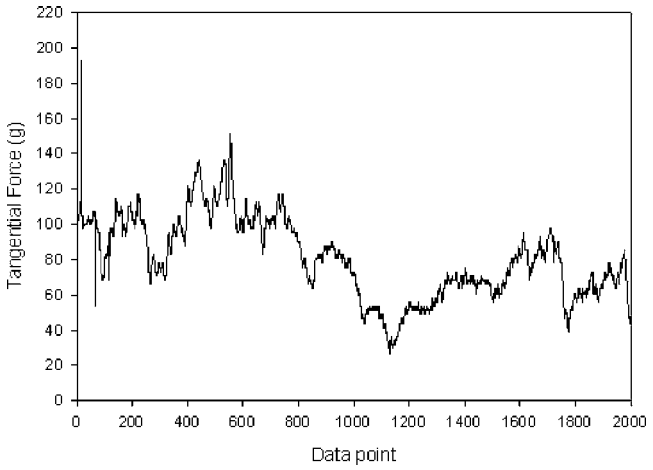

FIG. 2. Typical signal from the tribometer. The effective spring constant of the apparatus is 1 g/μm, giving the largest force drops as a few hundred μm.

measured with equal time intervals Δt is defined as follows:

$$S(f) = \left\langle \sum_{k=1}^{N} F(t_k) e^{2\pi i t_k f/N} \sum_{j=1}^{N} F(t_j) e^{-2\pi i t_j f/N} \right\rangle,$$

where $t_k = t_0 + k\Delta t$, $N = 2^n$ determines the size of the observation window, and $\langle \cdots \rangle$ denotes averaging over many nonoverlapping windows starting at different positions t_0. It must be emphasized that in this equation $F(t)$ represents not the force drop or slide jump but the original force or displacement.

We divide the original data (2^{19}) into 2^8 statistically independent nonoverlapping data sets of $N = 2^{11}$ points each. Next, we calculate 2^8 individual power spectra and finally average them to obtain the resulting power spectrum. Specific double-logarithmic plots are shown in Figs. 7–10. The

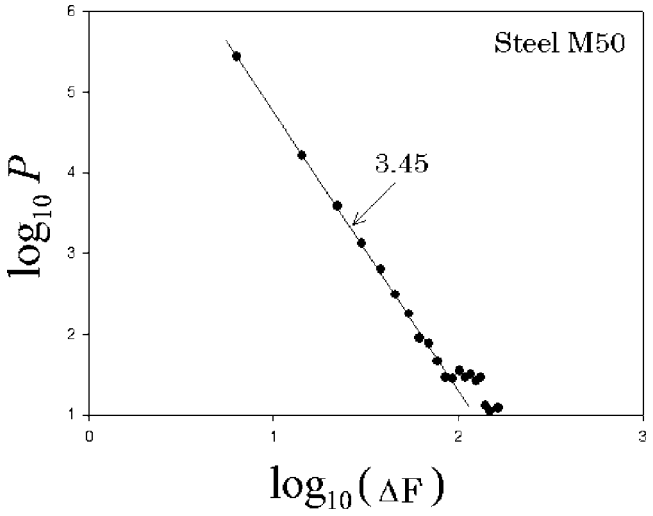

FIG. 3. Probability density for drop size distribution on steel M50.

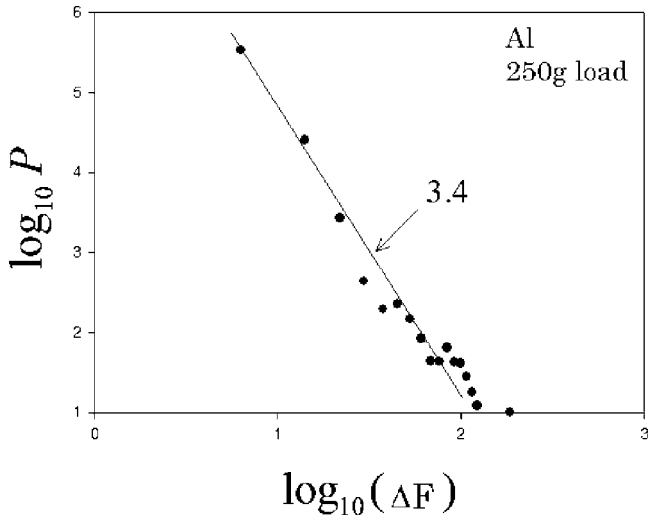

FIG. 4. Probability density for drop size distribution on aluminum with a normal load of 250 g.

power spectra follow power laws with exponents $1.0 \leqslant \alpha \leqslant 1.8$. The results of the probability distribution and power spectra analysis are summarized in Table I.

III. THEORY

A. Classical Robin Hood model

The model consists of a d-dimensional lattice. Each site i on this lattice at any time step n is characterized by the height $h_i(n)$ which we assume to be the height of an atomic-scale asperity at a given point of the interface between two bodies in contact. Here we present the one-dimensional case, which is an appropriate choice to model sliding friction but the analytical treatment is the same in any dimension, although the physically relevant cases are only $d=1$ and $d=2$. As the bodies slide against each other, the asperity with the maximal height is destroyed and some random number of atoms from this asperity is distributed among the neighboring asperities. To be specific, at each time step the site m

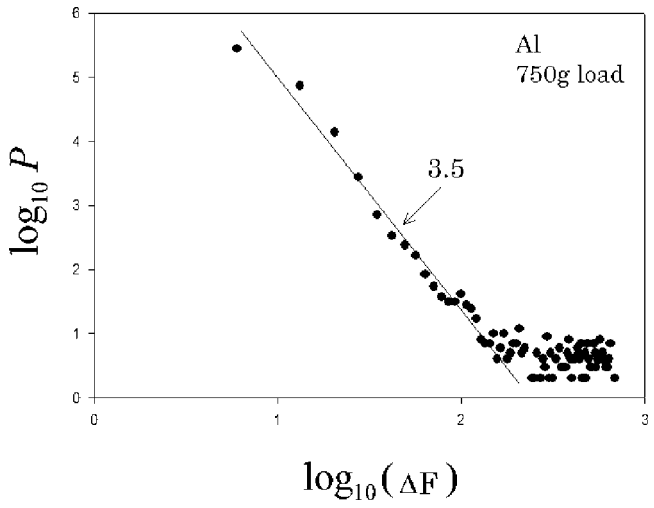

FIG. 5. As in Fig. 4 with normal load of 750 g.

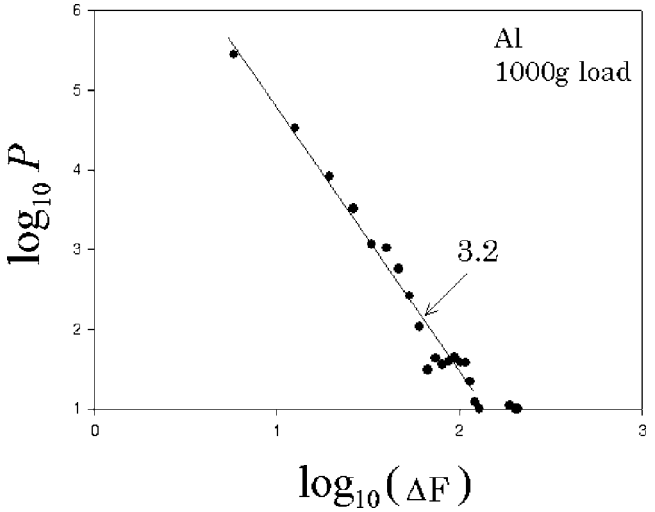

FIG. 6. As in Fig. 4 with normal load of 1000 g.

with maximal height $h_m(n)=\max h_i(n)$ is found and the new heights are determined according to the following rule: $h_m(n+1)=h_m(n)-r(n)$ and $h_{m\pm1}(n+1)=h_{m\pm1}(n)+r(n)/2$, where $r(n)$ are independent random variables uniformly distributed between 0 and 1. [Robin Hood determines the richest merchant in the market, robs him by a random amount $r(n)$, and distributes it equally among the neighbors without leaving anything for himself.] If we assume periodic boundary conditions so that the sites with $i=0$ and $i=L$ are equivalent, the total amount of matter $\Sigma_{i=0}^{L}h_i(n)$ is conserved and we can assume it to be zero. The distance between the surfaces at a given site i can be determined as $h_m(n)-h_i(n)$.

The particular details of the model such as the distribution of $r(n)$ or the rule of dividing it among neighbors can vary, but the model still retains its SOC behavior. The critical exponents appear to be sensitive to the details of dividing $r(n)$; for example, an exactly solvable asymmetric model (in which all the profit is given to the site on the left) [41] belongs to a different universality class.

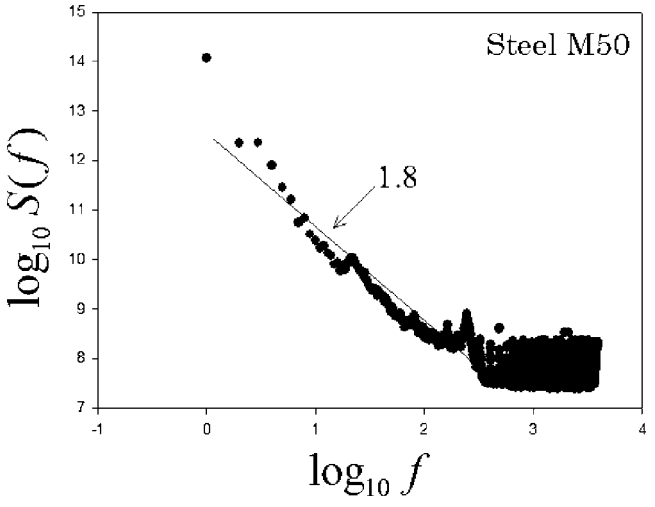

FIG. 7. Power spectrum of the signal from the tribometer (force time series) for a steel M50 sample.

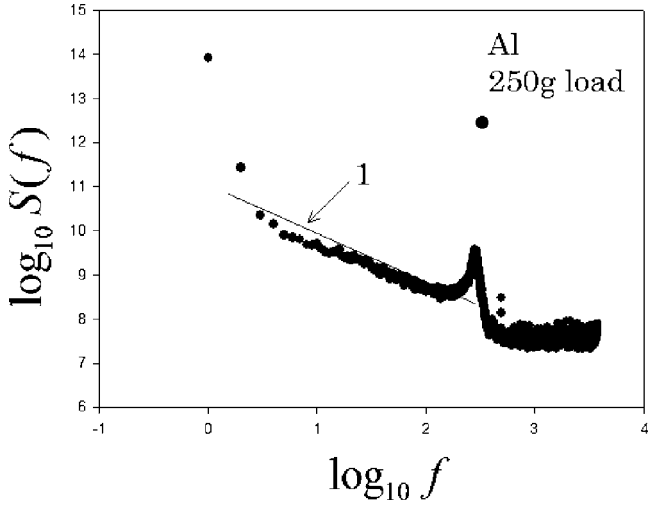

FIG. 8. Power spectrum of the signal from the tribometer (force time series) for an aluminum sample with a normal load of 250 g.

It has been shown [42,43] that in a wide class of depinning SOC models, all the critical exponents can be expressed in terms of the two main exponents: avalanche dimension D and correlation exponent ν. The avalanche of threshold h_0 is defined as a sequence of time steps during which the height of the maximal asperity is above h_0. Namely, if $h_m(n_0)\leqslant h_0$ and $h_m(n_0+s)\leqslant h_0$ while for $n_0<n<n_0+s$, $h_m(n)>h_0$, the sequence $n=n_0+1,\ldots,n_0+s$ is called a punctuating avalanche of threshold h_0 and mass s. The avalanche dimension describes how the avalanche mass s scales with the horizontal dimension of the avalanche R. To be more precise, the mass distribution of avalanches with threshold h_0 scales as

$$P_s(s) \sim s^{-\tau_s} g_s(s(h_0-h_c)^{D\nu}) \tag{1}$$

and the distribution of the avalanche horizontal size R scales as

$$P_R(R) \sim R^{-\tau_R} g_R(R(h_0-h_c)^{\nu}), \tag{2}$$

where $h_c \approx 0.114$ is the critical height,

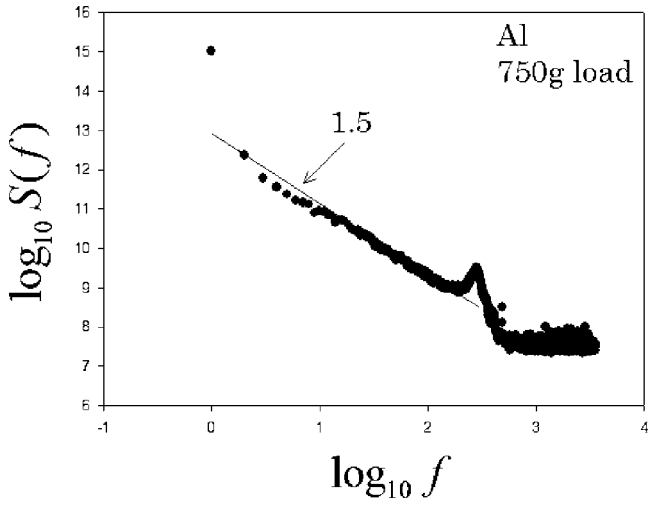

FIG. 9. As in Fig. 8 with a normal load of 750 g.

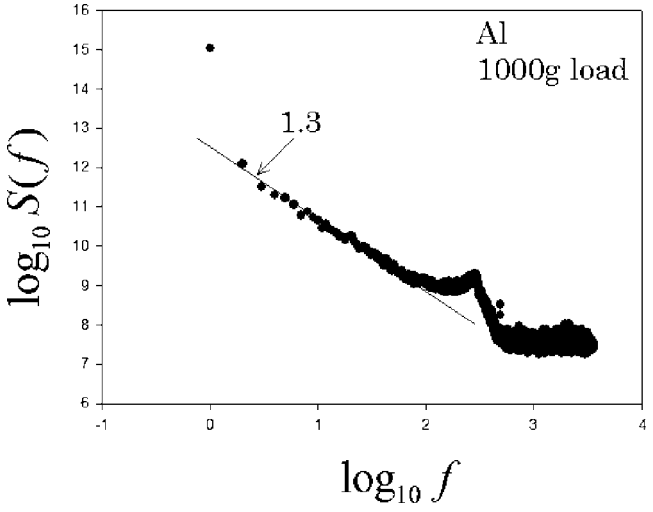

FIG. 10. As in Fig. 8 with a normal load of 1000 g.

$$\tau_s = 1 + (d - 1/\nu)/D, \tag{3}$$

and

$$\tau_R = 1 + d - 1/\nu \tag{4}$$

are Fisher exponents first introduced to characterize cluster distributions in percolation theory [44], while g_s and g_R are exponentially decreasing cutoff functions. It has been suggested [45] that the Robin Hood model belongs to the same universality class as the linear interface model, for which the values ($D=2.23$ and $\tau_s=1.13$ in $d=1$, $D=2.725$ and $\tau_s=1.29$ in $d=2$) are given in Ref. [43]. Using these values and Eq. (3), one gets $\nu=1.41$ for $d=1$ and $\nu=0.83$ for $d=2$.

It can be shown that after the initial equilibration number of time steps $T \sim L^D$, any initial shape of the interface $h_i(0)$ reaches a steady state such that very few $N(L)$ "rich" sites have $h_i(n) > h_c \approx 0.114$, where

$$N(L) \sim L^{d_f} \tag{5}$$

and

$$d_f = d - 1/\nu \tag{6}$$

plays the role of fractal dimension of rich sites. Only those few rich sites have a chance to be robbed. The chance $P_m(h_m)$ that at a given time step the maximal height is equal to h_m decreases for an infinite system [42] as

TABLE I. The values of exponents μ characterizing the power law behavior of the distribution of the force-drop sizes and spectral exponents α characterizing the power spectrum of the friction force time series for different materials and loads.

Material	Load (g)	μ	α
M50	1000	3.5	1.8
Al	250	3.4	1.0
Al	750	3.5	1.5
Al	1000	3.2	1.3

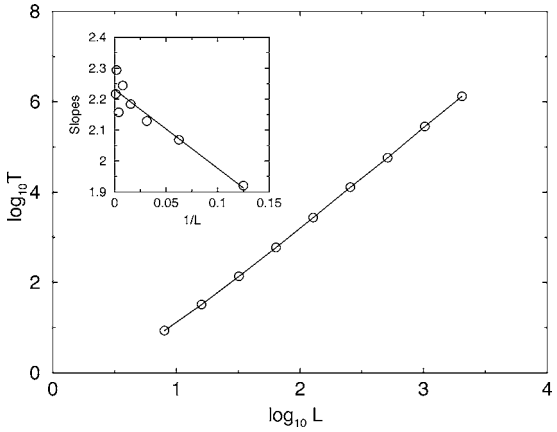

FIG. 11. Double-logarithmic plot of the average equilibration time $\langle T \rangle$ versus system size $L=2^3, 2^4, \ldots, 2^{12}$. The inset shows the successive slopes of the main graph versus $1/L$. The intercept $D=2.23$ agrees with the data of Ref. [43].

$$P_m(h_m) = (h_m - h_c)^{\gamma - 1}, \tag{7}$$

where the exponent

$$\gamma = 1 + \nu(D - d) \tag{8}$$

characterizes the dependence of the average avalanche size on its threshold h_0: $\langle s \rangle \sim (h_0 - h_c)^{-\gamma}$.

The distribution of heights of the poor sites converges to a smooth distribution on the interval $[h_c - 1, h_c]$, while the distribution of the rich sites converges to the distribution with a power law singularity

$$P_h(h) \sim (h - h_c)^{-d\nu}. \tag{9}$$

This result is not presented in Refs. [42,43] but can be justified by the following heuristic arguments. Indeed, the number of sites with $h > h_0$ scales as the number of the active sites in an avalanche of threshold h_0 and thus scales as $R^{d_f}(h_0)$, where $R(h_0)$ is the cutoff of the avalanche distribution (2) which scales as

$$R(h_0) \sim (h_0 - h_c)^{-\nu}. \tag{10}$$

Thus the probability that $h > h_0$ scales as $(h_0 - h_c)^{-d_f\nu}$ and the probability density of $h = h_0$ scales as

$$P_h(h_0) \sim (h_0 - h_c)^{-d_f\nu - 1} = (h_0 - h_c)^{-d\nu}. \tag{11}$$

In order to illustrate these theoretical predictions, we perform simulations of the one dimensional Robin Hood model. Starting at $n=0$ with a flat interface $h_i(0)=0$, electing the first site to rob at random, after T steps we get all L sites of the interface updated at least once. Measuring the average $\langle T \rangle$ for many independent runs for different system sizes, and plotting it versus L in a log-log scale (Fig. 11), we can obtain the avalanche dimension D as the limit of the successive slopes of this graph for $L \to \infty$. In fact, the behavior of the model does not depend on the initial condition. It can be shown that for any values of $h_i(0)$ the system will

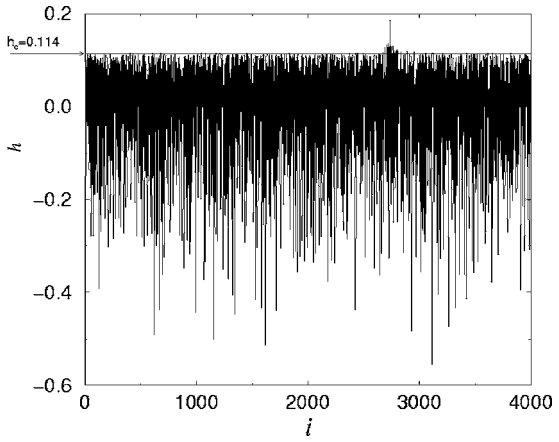

FIG. 12. A typical shape of the steady-state interface $h_i(n)$ for $n \gg \langle T \rangle$. The horizontal axis i is the coordinate along the interface. The vertical axis represents the normal coordinate of the relative surface profile. The distance between the surfaces at each point is assumed to be equal $h_m - h_i$, where h_m is the maximal value of h_i, which for this particular realization (h_m=0.185) is reached for i=2737. The horizontal line shows the critical height.

reach the critical state after the same average relaxation time $\langle T \rangle \sim L^D$. This critical state corresponds to the actual topography of the interfaces during sliding.

A typical shape of the interface at time $n > T$ is presented in Fig. 12. One can see that the height of the majority of sites does not exceed the critical value $h_c \approx 0.114$. Interestingly, the majority of rich sites with heights above the critical barrier are localized in the vicinity of the richest site.

Figure 13 shows the histogram of all the interface heights $P_h(h)$ collected over many time steps after the system has reached the steady state and the histogram of the heights of the robbed sites $P_m(h_m)$. One can see that while $P_h(h)$ dramatically increases as $h \to h_c^+$, no sites below the critical value are robbed and $P_m(h_m) \to 0$ as $h_m \to h_c^+$. In order to find the exponents governing the behavior of these distributions near the critical point, we plot these quantities in a double-logarithmic scale as functions of $h - h_c$ [Fig. 13(b)] and find good agreement between their slopes and the exponents predicted by the Eqs. (9) and (7).

B. Relating the Robin Hood model to dry friction

Imagine the landscape of Fig. 12 to be a profile of one of the interfaces (the bottom one) which touches the flat interface at the top by its highest asperity. (In fact, we can assume that both of the interfaces are rough and the distance between the two interfaces at a given point i is given by $h_m - h_i$.) As the interfaces are moving against each other, h_m fluctuates, sometimes increasing and sometimes decreasing almost to the critical value h_c. When h_m is high, then only one asperity creates a contact between the interfaces and the friction force is small. If h_m is close to h_c, many asperities are within the range of atomic forces with the opposite interface and the friction force is large. Thus, we assume that the friction force $F(n)$ at a given time step is proportional to the number $P_h(h_m(n))\Delta h$ of asperities with heights between $h_m(n) - \Delta h$ and $h_m(n)$:

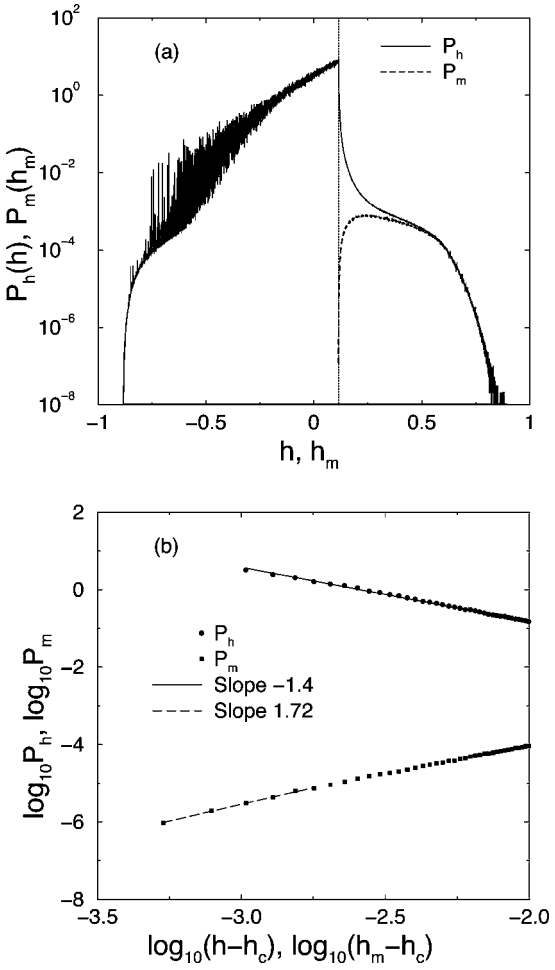

FIG. 13. (a) The semilogarithmic plot of the distribution of heights $P_h(h)$ of all sites (solid line) and the distribution of heights $P_m(h_m)$ of robbed sites (dashed bold line). The vertical dotted line shows the position of the critical height h_c=0.114. (b) Double-logarithmic plot of the same quantities plotted as functions of $h - h_c$. The slopes of the curves in the fitted regions are in agreement with Eq. (9), $-d\nu = -1.4$, and Eq. (7), $\nu(D-1) = 1.72$.

$$F(n) = F_1 P_h(h_m(n))\Delta h, \tag{12}$$

where Δh is the interaction distance of atomic forces acting between the two surfaces and F_1 is a proportionality coefficient, corresponding to the surfaces interaction force at the asperity. Accordingly, the distribution of the friction forces $P(F)$ satisfies the equation $P(F)dF = P_m(h_m)dh_m$, where the random variables F and h_m are linked by Eq. (12). Taking into account Eqs. (9) and (12) we have $dh_m/dF \sim dF^{-1/d\nu}/dF \sim F^{-1/d\nu - 1}$. Finally Eq. (7) yields

$$P(F) = P_m(h_m(F))\frac{dh_m}{dF} \sim F^{-(\gamma-1)/d\nu} F^{-1/d\nu - 1} = F^{-\mu}, \tag{13}$$

where

$$\mu = (D + 1/\nu)/d. \tag{14}$$

Since the distribution of the difference between two power-law-distributed random variables also has a power law tail,

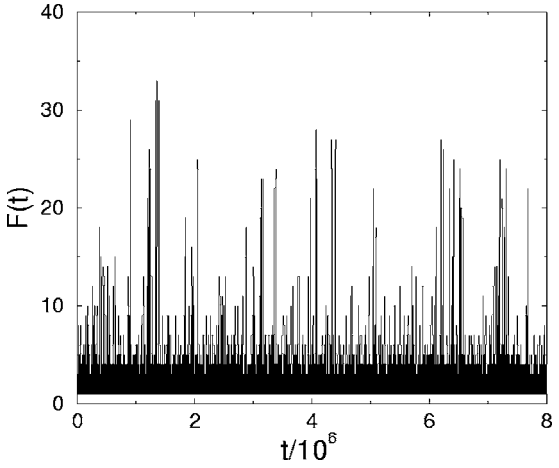

FIG. 14. Time series of $F(t)$ for $L=4096$, $\Delta h=2^{-10}$.

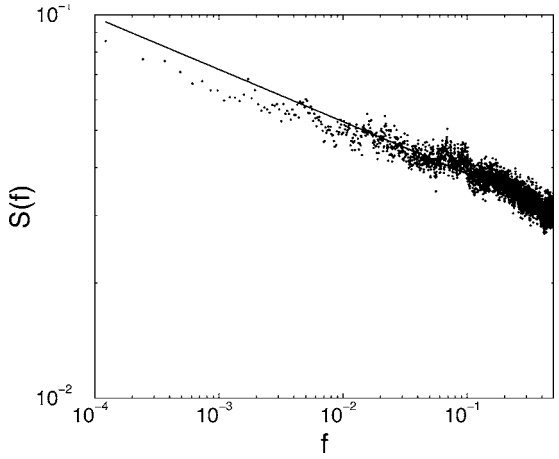

FIG. 16. Power spectrum of the time series $F(t)$ presented in Fig. 14. The slope of the straight-line fit is $-\alpha=-0.14$.

the distribution of the negative force drops ΔF scales as $\Delta F^{-\mu}$ with the same exponent μ.

For $d=1$, using values of Ref. [43] we have $P(F)\sim F^{-\mu}$ with $\mu=2.94$ which is consistent with the experimental observations of the density of the force-drop sizes presented here and in Ref. [46]. For $d=2$ we have $\mu=1.96$.

For the one-dimensional Robin Hood model we determine the time series of forces, defined as the number of heights between $h_m(n)$ and $h_m(n)-\Delta h$ as a function of time (Fig. 14). The histogram of the negative force drops for this time series is presented in Fig. 15 in a double-logarithmic scale. The slope of this plot is $-\mu=-3.0$, which is consistent with the theoretical prediction (14).

Note that the time series $F(n)$ is slightly correlated, which can be demonstrated by the negative slope of its power spectrum $S_F(f)\sim f^{-\alpha}$ in the log-log scale (Fig. 16). The explanation of this phenomenon is based on the fact that the values of $h_m(n)$ fluctuate in the vicinity of h_c in a nontrivial way, so that $h_m(n)$ become less than $h_c+\epsilon$ at time steps n separated by intervals distributed according to Eq. (1). This is because these intervals coincide with avalanches for the threshold $h_0=h_c+\epsilon$. The values of $h_m(n)$ below $h_c+\epsilon$ correspond to the large values of forces $F(n)$, and thus the intervals between the forces $F(n)$ above certain threshold are also distributed according to Eq. (1). It can be shown [43,47] that the exponent α of a time series generated by peaks separated by intervals of zero signal distributed according to a power law as in Eq. (1) is equal to τ_s-1 for $1<\tau_s<2$. Thus, according to Eq. (3), $\alpha=\tau_s-1=(d-1/\nu)/D\approx 0.13$. Indeed, the numerical data of Fig. 16 give $\alpha\approx 0.14$, in a very good agreement with the above theoretical prediction. However, this value of the spectral exponent is much smaller than the values observed experimentally which are in the range between 1.0 and 1.8.

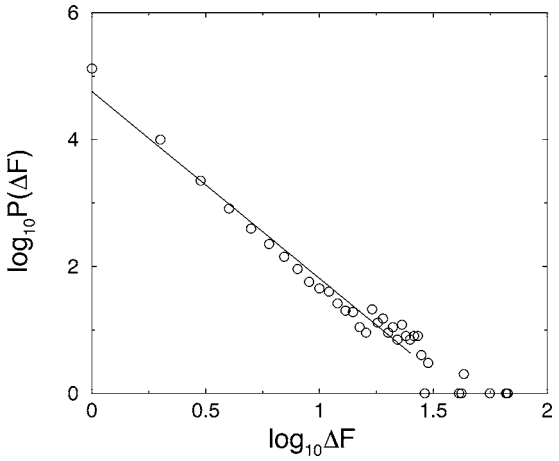

FIG. 15. Distribution of forces drops, $P_F(\Delta F)$, for $L=8192$, $\Delta h=2^{-10}$. The slope of the straight-line fit is $-\mu=-3$.

This difference is to be expected since the materials in contact as well as the strain gauge have finite elastic constants and inertia which produce a time delay between the applied force and the displacement recorded by the tribometer and therefore lead to an effective integration of the input force time series. If real materials were infinitely stiff, then the experimental force power spectrum should agree with the theoretical predictions. To compare with realistic situations, we construct a mechanical model of a tribometer that accounts for these effects.

C. Introducing the effects of the tribometer

As in the Tomlinson model [29], we assume that the pin of the tribometer contacts the sample at time t at a point with coordinate $x(t)$ and it is dragged along the sample by the strain gauge spring with constant k attached to the body of the instrument moving along the sample with constant velocity v_0, which is equivalent to the rotational speed of the disk. The force measured by the tribometer is thus $k[v_0t-x(t)]$, which fluctuates as the pin moves against the sample with velocity $v(t)=dx/dt$ and acceleration $a(t)=d^2x/dt^2$. The equation of motion of the pin is thus

$$ma = (v_0 t - x)k - F(t,v), \tag{15}$$

where $F(t,v)$ is the friction force generated by the asperities of the sample and m is the mass of the pin. In the Tomlinson model, $F(t,v)$ is the force created by the periodic potential which models the atomic forces. In our case, it is created by the random force $F(n)$ created by many asperities distributed across the sample as described in the previous section.

Now our goal is to relate $F(t,v)$ with the input from the Robin Hood model $F(n)$. Note that the physical time t is not directly proportional to the time step n of the Robin Hood model, but is equal to the sum of the durations of each time step,

$$t = \sum_{i=1}^{n} t_i, \tag{16}$$

where the durations t_i are the times needed for the pin to travel a characteristic distance Δx, which is the linear size of each asperity. It can be also related to the critical displacement needed to destroy the highest asperity. We assume that if the pin moves along the sample by Δx, the current asperity is destroyed and the landscape of the contact between the pin and the sample is rearranged according to the rules of the model. Thus the time step n_t of the Robin Hood model, corresponding to a given moment of time t, can be determined as

$$n_t = \text{int}[x(t)/\Delta x], \tag{17}$$

where int[...] denotes the integer part of the expression in the brackets.

Once we know n_t as a function of t we can define $F(t,v)$ as

$$F(t,v) = \begin{cases} \text{sgn}(v_0 t - x)\min(bF(n_t), k(v_0 t - x)), & v = 0, \\ \text{sgn}(v)[bF(n_t) + \eta v], & v \neq 0, \end{cases} \tag{18}$$

where $F(n_t)$ is the input from the Robin Hood model, and $\eta > 0$ is a dissipative constant. The constant b depends on the elastic properties of the material. Introducing dimensionless variables by $x' = x/\Delta x$ and $t' = tv_0/\Delta x$, we arrive at a dimensionless equation

$$a' = (t' - x')k' - F'(t',v'), \tag{19}$$

where $k' = k\Delta x^2/mv_0^2$ and $F'(t',v')$ is the same as $F(t,v)$ but the constants b and η are changed by $b' = b\Delta x/mv_0^2$ and $\eta' = \eta\Delta x/mv_0$.

Thus, there are three independent dimensionless parameters of the model: k', b', and η'. Varying these parameters, we found a wide region in the parameter space in which the power spectrum of the model resembles the experimental one. A typical example of the spectrum is shown in Fig. 17. The frequency of the resonance peak is determined by $\sqrt{k'}/2\pi \approx 5 \times 10^{-3}$. The peak becomes more pronounced as we decrease η'. The increase in η' also increases the slope of the spectrum. The increase of b' at given k' increases the frequency region in which the power spectrum follows the power law but it also increases the absolute value of the slope closer to 2, a characteristic value of Brownian motion. Interestingly, the large value of the spectral exponent found for steel, can be associated with the larger strength of the asperities which is modeled by the parameter b.

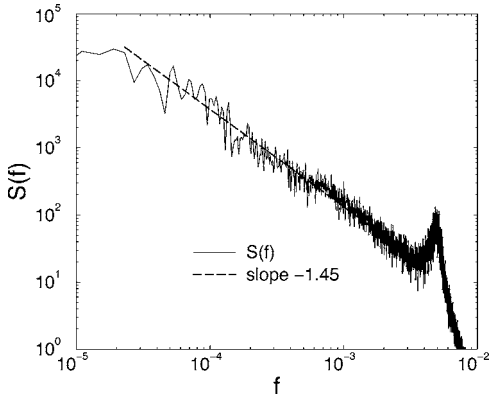

FIG. 17. Power spectrum of the time series produced by Eq. (19) for $k' = 0.001$, $b' = 0.3$, and $\eta' = 0.01$.

In general, an integration of the time series corresponds to the increase of the spectral exponent by 2, so integration of the white noise produces Brownian noise. The observed spectral exponent $\alpha = 1.45$ suggests that in a certain range of parameters, our model acts as the fractional integrator of the input signal. For a very stiff spring and large dissipation ($k=1$, $b=0.1$, $\eta=1$) the output signal of our equation is not much different from the input time series $F(n_t)$ and we recover the small value of the spectral exponent $\alpha = 0.14$. Note that the parameters of the tribometer—inertia m, stiffness k, load b, and dissipation η—do not change the input to the tribometer which is a power-law-distributed noise $F(n)$. Thus one can expect that the large force drops can be still visible at the output of the tribometer, which cannot filter out large and rare events. Figure 18 shows the distribution of the force

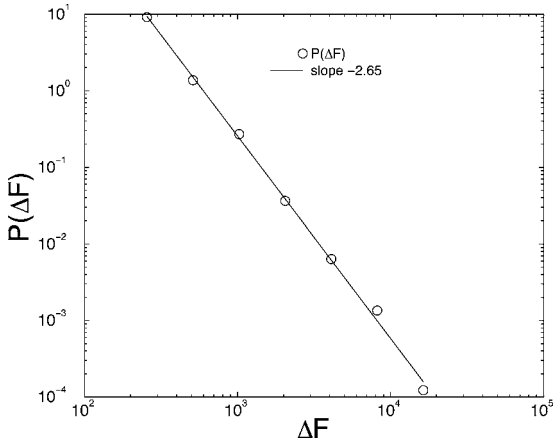

FIG. 18. Distribution of the measured force drops, $P_F(\Delta F)$, for the tribometer model with $k' = 0.001$, $b' = 0.3$, and $\eta' = 0.01$.

drops measured by the tribometer with the same parameters as in Fig. 17. One can see that the distribution is still a power law with the exponent $\mu \approx 3$ as in the input time series (Fig. 15). This is supported by the universal value $\mu \approx 3.4$ found in experiments, which does not depend on the load and material.

IV. DISCUSSION

In the previous section we have explored in detail an improved version of the one-dimensional Robin-Hood model. Friction is a two-dimensional phenomenon, and one can argue that the one-dimensional model is not sufficient to describe friction. That is why we also investigate the two-dimensional Robin-Hood model, in which the mass taken from the highest asperity is distributed equally among its four neighbors. Using known values of the critical exponents of the two-dimensional Zaitsev model [43] we predict the value of the exponent $\mu=1.96$ describing the distribution of the force drops.

Two surfaces in contact correspond to a two-dimensional situation, but we have found that the $d=1$ case provides better fit to the experimental results. We propose that this might be due to a process of integrating out the degrees of freedom perpendicular to the direction of the relative motion. Specifically, one can view the quantity $h(i)$ either as an average (in the direction perpendicular to the motion) of the corresponding $h(i,j)$—that is, $h(i)=\Sigma_j h(i,j)$—or $h(i)=\max_j h(i,j)$.

Also, it is clear that one can expect a strong anisotropy in mass redistribution due to the directionality of the motion which is one dimensional. It is known that even in the one-dimensional case the anisotropy of redistribution plays a significant role and changes the critical exponents of the Robin Hood model, giving $\mu=2$. These facts show that both dimensionality and anisotropy may play a role in the values of the exponent μ and thus deserve a separate study which is beyond the scope of the present paper, the goal of which is to propose a way of relating an extremal dynamics and friction which involves wear.

The relationship between that force drop and the drop in the number of asperities creating atomic contacts between the sliding surfaces provides a direct mechanism of how the creeping dynamics of Zaitsev's model maps into a real dynamics. In fact the number of asperities which are responsible for creating the adhesive forces between the interfaces is not proportional to h_m but is a decreasing function of h_m, reaching its maximum when h_m approaches the critical threshold.

The power law distribution of force drops comes not from the elastic interaction in the sliding chain as in the Lacombe model, but from the fluctuation in the number of the asperities between the interfaces which creates a power law noise microscopic input in the macroscopic mechanical model. Thus, in our approach, the stiffness and inertia do not play the explicit role in the formation of the avalanches as in the Lacombe model. In our approach, they can only integrate the effect of the microscopic power-law-distributed input. Indeed, as our simulations show, the power law distribution of the large force drops remains intact in the vast region of the parameter space. But we show that the stiffness and inertia may significantly change the power law spectrum behavior.

Although our model can explain the experimental results, it is reasonable to question the absence of elasticity in our interpretation of the extremal dynamics of the Robin Hood model, which serves as a microscopic input to our model of the tribometer. The Tomlinson-like model of the tribometer is the only place in our approach where elasticity is taken into account. As presented by Caroli and Nozieres [17], elasticity is one among other mechanisms (adhesion, plastic flow of asperities) relevant for friction. They show that despite its long range, it plays a minor role in the solid friction of multicontact interfaces, like the situation we studied. Thus, although present and relevant to friction in general, elasticity plays a minor role in dry friction stick-slip.

V. CONCLUSIONS

We have presented experimental results and theoretical arguments that support the presence of self-organized criticality in dry sliding friction. The experiments are pin-on-disk friction force traces of aluminum-aluminum and steel-steel systems. In both cases and for a variety of normal loads, the probability distribution of the friction force drops and the frequency power spectra are power laws. The values of the exponent $\mu=3.4\pm0.5$ is much larger than the value obtained in Ref. [12] for artificially constructed elastic interfaces. In addition, the force-drop and power-spectrum exponents are load independent. Although further studies including a larger range of loads and materials are necessary, these results suggest the interesting possibility of universal exponents.

The theoretical arguments are based on the application of the Robin Hood model to the friction problem. This model provides rules by which the surface profile changes as a function of time (Sec. III B). The model introduces a height h that we interpret physically as the height of the asperity. At each time step, atoms from the highest asperity are distributed among neighboring sites. We use the known distribution of heights and of maximal heights h_m of the Robin Hood model to obtain the time series of the friction forces created by the asperities. As the maximum height fluctuates near the critical value, the number of smaller asperities whose heights are within the reach of atomic forces also fluctuates, diverging as h_m comes close to the critical value h_c. These smaller asperities correspond to the contact sites and are responsible for the friction force. Specifically, the friction force is proportional to the number of contacts. Thus we propose that the friction force at a given time step is proportional to the probability density of the interface heights at the current value of the maximal height. The statistical distribution of the friction forces is studied both numerically and analytically.

We also find that the large forces are bunched in time. This is due to fluctuations of the maximal heights above a

constant critical height. When the maximum heights return to the critical value, the forces become large. Thus, the surface waxes and wanes between a situation of large force due to many asperities acting and a situation of smaller force in which only few asperities are in contact.

In addition, we use the time series of forces as an input to the Newton's equation which describes the kinematics of the pin (Sec. III C). For stiff or massless materials, the experimental distribution of force drops should coincide with the theoretical distribution of forces. However, materials have finite mass and elasticity and thus the experimentally measured friction forces differ from the actual forces at the contact. To investigate these effects, we solve this equation numerically for different values of the parameters and find good agreement with the experiment.

Extremal dynamics models (such as the Robin Hood model utilized in this work) are more than a decade old and could be seen as primitive. However, we believe that they still have an underutilized potential for understanding friction. In fact the only alternative approach to them is the elastic chain model, which is essentially one dimensional and can be mapped onto an extremal dynamics model in the limit of slow driving velocity. The elastic-chain model emphasizes the elastic interactions between the elements of the sliding interface, assuming some interaction potential with randomly distributed asperities. Our interpretation of the Robin Hood model emphasizes the nonelastic friction which involves wear and mass transfer between the neighboring asperities. The difference in the predictions of these two approaches regarding the force-drop distribution exponent μ must be further tested experimentally in the absence and presence of wear.

ACKNOWLEDGMENTS

S.V.B. thanks Yeshiva University for providing the high-performance computer cluster that made this work possible. F.R.Z. acknowledges support by Research Corporation through Grant No. CC5786. F.R.Z. and J.F. thank Phillip Abel, Mark Jansen, and Kathleen Scanlon of NASA-Glenn Tribology Group for collaboration in the initial stages of this project.

[1] R. Hallgass, V. Loreto, O. Mazzella, G. Paladin, and L. Pietronero, Phys. Rev. E **56**, 1346 (1997).
[2] F.-J. Elmer, Phys. Rev. E **56**, R6225 (1997).
[3] R. V. Sole and S. C. Manrubia, Phys. Rev. E **54**, R42 (1996).
[4] V. Plerou, P. Gopikrishnan, L. A. Nunes Amaral, M. Meyer, and H. E. Stanley, Phys. Rev. E **60**, 6519 (1999).
[5] O. Peters, C. Hertlein, and K. Christensen, Phys. Rev. Lett. **88**, 018701 (2002).
[6] F. Slanina, Phys. Rev. E **59**, 3947 (1999).
[7] S. Ciliberto and C. Laroche, J. Phys. I **4**, 223 (1994).
[8] D. P. Vallette and J. P. Gollub, Phys. Rev. E **47**, 820 (1993).
[9] P. Bak, C. Tang, and K. Wiesenfeld, Phys. Rev. Lett. **59**, 381 (1987).
[10] H. J. Jensen, *Self-Organized Criticality: Emergent Complex Behavior in Physical and Biological Systems, Cambridge Lecture Notes in Physics*, No. 10 (Cambridge University Press, London, 1998).
[11] D. L. Turcotte, Rep. Prog. Phys. **62**, 1377 (1999).
[12] S. Ciliberto and C. Laroche, J. Phys. I **4**, 223 (1994).
[13] S. Ciliberto and C. Laroche, Eur. Phys. J. B **9**, 551 (1999).
[14] E. Gnecco, R. Bennewitz, T. Gyalog, Ch. Loppacher, M. Bammerlin, E. Meyer, and H.-J. Güntherodt, Phys. Rev. Lett. **84**, 1172 (2000).
[15] F. P. Bowden and D. Tabor, *The Friction and Lubrication of Solids* (Clarendon Press, Oxford, 1950).
[16] B. N. J. Persson, *Sliding Friction* (Springer, Berlin, 1998).
[17] C. Caroli and Ph. Nozieres, Eur. Phys. J. B **4**, 233 (1998).
[18] J. A. Harrison, C. T. White, R. J. Colton, and D. W. Brenner, J. Phys. Chem. **97**, 6573 (1993).
[19] J. A. Harrison, C. T. White, R. J. Colton, and D. W. Brenner, Thin Solid Films **260**, 205 (1995).
[20] R. Komanduri, N. Chandrasekaran, and L. M. Raff, Phys. Rev. B **61**, 14007 (2000).
[21] J. Cai and J. S. Wang, Phys. Rev. B **64**, 113313 (2001).
[22] O. A. Mazyar, H. W. Xie, and W. L. Hase, J. Chem. Phys. **122**, 094713 (2005).
[23] J. Zhong, J. B. Adams, and L. G. Hector, J. Appl. Phys. **94**, 4306 (2003).
[24] T. Ohzono and M. Fujihira, Phys. Rev. B **62**, 17055 (2000).
[25] P. T. Mikulski and J. A. Harrison, J. Am. Chem. Soc. **123**, 6873 (2001).
[26] P. T. Mikulski, G. Gao, G. M. Chateauneuf, and J. A. Harrison, J. Chem. Phys. **122**, 024701 (2005).
[27] L. Zhang and S. Jiang, J. Chem. Phys. **117**, 1084 (2002).
[28] Q. Zhang, Y. Qi, L. G. Hector, T. Cagin, and William A. Goddard III, Phys. Rev. B **72**, 045406 (2005).
[29] E. Gnecco, R. Bennewitz, T. Gyalog, and E. Meyer, J. Phys.: Condens. Matter **13**, R619 (2001).
[30] A. Schirmeisen, L. Jansen, and H. Fuchs, Phys. Rev. B **71**, 245403 (2005).
[31] C. Fusco and A. Fasolino, Phys. Rev. B **71**, 045413 (2005).
[32] P. Reimann and M. Evstigneev, Phys. Rev. Lett. **93**, 230802 (2004).
[33] M. Evstigneev and P. Reimann, Phys. Rev. E **71**, 056119 (2005).
[34] S. Y. Krylov, K. B. Jinesh, H. Valk, M. Dienwiebel, and J. W. M. Frenken, Phys. Rev. E **71**, 065101(R) (2005).
[35] F. Lacombe, S. Zapperi, and H. J. Herrmann, Phys. Rev. B **63**, 104104 (2001).
[36] D. Cule and T. Hwa, Phys. Rev. B **57**, 8235 (1998).
[37] D. Cule and T. Hwa, Phys. Rev. Lett. **77**, 278 (1996).
[38] S. I. Zaitsev, Physica A **189**, 411 (1992).
[39] S. Roux and E. Guyon, J. Phys. A **22**, 3693 (1989).
[40] P. Bak and K. Sneppen, Phys. Rev. Lett. **71**, 4083 (1993).
[41] S. Maslov and Y.-C. Zhang, Phys. Rev. Lett. **75**, 1550 (1995).
[42] S. Maslov, Phys. Rev. Lett. **74**, 562 (1995).

[43] M. Paczuski, S. Maslov, and P. Bak, Phys. Rev. E **53**, 414 (1996).
[44] D. Stauffer and A. Aharony, *Introduction to Percolation Theory* (Taylor & Francis, Philadelphia, 1994).
[45] S. Roux and A. Hansen, J. Phys. I **4**, 515 (1994).
[46] F. R. Zypman, J. Ferrante, M. Jansen, K. Scanlon, and P. Abel, J. Phys.: Condens. Matter **15**, L191 (2003).
[47] S. B. Lowen and M. C. Teich, Phys. Rev. E **47**, 992 (1993).